RSC Advances

PAPER

View Article Online
View Journal | View Issue

Cite this: *RSC Adv.*, 2024, **14**, 4835

Fe-modified NASICON-type $Na_3V_2(PO_4)_3$ as a cathode material for sodium ion batteries

Shuling Liu, *[ab] Zheng Xu,[ab] Lei Ren,[ab] Wenxuan Xu,[ab] Yuan Liu,[ab] Xuanlu Fan,[ab] Muxuan Luo,[d] Jiebing Li[c] and Jianbo Tong *[ab]

Received 21st December 2023
Accepted 16th January 2024

DOI: 10.1039/d3ra08714j

rsc.li/rsc-advances

The sol–gel method is used to synthesize a new compound called $Na_3Fe_{0.8}V_{1.2}(PO_4)_3$/C (NFVP/C), which has a crystal structure and belongs to the NASICON-type family. The dimensions of NFVP's unit cell are a = 8.717 (1) Å, c = 21.84 (1) Å, and V = 1437.27 (0) Å3. The Na||NFVP/C battery provides a discharge potential of 3.43 V compared to Na^+/Na, an intriguing rate capability of 76.2 mA h g^{-1} at 40C, and maintains an impressive capacity of 97.8% after 500 cycles at 5C. The excellent efficiency of $Na_3Fe_{0.8}V_{1.2}(PO_4)_3$/C can be ascribed to its elevated Na+ conductivity and reduced energy barrier for sodium-ion diffusion. The NASICON-type $Na_3Fe_{0.8}V_{1.2}(PO_4)_3$/C is a promising material for sodium-ion batteries.

1. Introduction

Given the possibility of energy deficits and ecological contamination, it is crucial to make progress in the development of alternative energy sources and storage methods.[1–3] Rechargeable batteries possess the capability to address the problem of storing energy derived from solar, wind, and other sustainable sources. Although the scarcity of lithium resources has led to a rise in the price of lithium-ion batteries, they continue to be widely used in electric vehicles, mobile phones, and laptop computers due to their exceptional energy density and long-lasting cycle life of.[4–7] Nevertheless, in order to address the rising cost of Li-ion batteries, it is imperative to explore alternative battery technologies that offer superior performance.

Due to their affordable price and abundant availability, sodium-ion batteries (SIBs) have attracted considerable attention.[8–10] However, the slow ion diffusion kinetics in the host material of Na^+ is caused by the significant ionic radius of sodium (1.02 Å) in comparison to lithium (0.76 Å), presenting a challenge to the battery's performance in terms of rate and stability during cycles. Despite the enhancement of transport kinetics at the electrode–electrolyte interface through electrolyte refinement, the crucial aspect still lies in developing electrode materials that are better suited for SIBs.[11–15]

Over the past few years, extensive research has been conducted on various cathode materials for sodium energy storage with possess open-framework structures,[16,17] such as transition metal oxides with layered/tunneled structures,[18–21] polyanionic compounds,[22–27] Prussian blue analogues,[28,29] and organic materials,[30] have been studied. $Na_3V_2(PO_4)_3$(NVP), a polyanionic phosphate of the NASICON type with a spacious three-dimensional structure and channels, is considered a highly promising cathode candidates for SIBs among others.[31] With a theoretical energy density of 370 W h kg^{-1}, favorable stability, and minimal volume expansion during electrochemical processes, $Na_3V_2(PO_4)_3$ emerges as a highly promising phosphate material for SIBs.[32,33] Nevertheless, the $Na_3V_2(PO_4)_3$ compound does not exhibit significant electronic conductivity, and enhanced electrochemical properties are primarily attained by incorporating ions and utilizing carbon capping techniques.[17,34–37] Furthermore, V is a costly and extremely poisonous element, thus cathode materials for SIBs need to be eco-friendly and affordable. The substantial quantity of V utilized poses a constraint for the sustainable progress and widespread implementation of $Na_3V_2(PO_4)_3$.[38] So far, there have been suggestions to improve the overall electrochemical efficiency of $Na_3V_2(PO_4)_3$ by utilizing cation doping in a restricted manner, including Cr^{3+},[39] Mn^{2+}/Mn^{3+},[40] Mg^{2+},[41] Mo^{6+},[42] Fe^{3+},[43] and Ti^{4+}.[44] According to Liu and colleagues by augmenting the quantity of Cr^{3+} in $Na_3V_2(PO_4)_3$, the synthesized compound $Na_3VCr(PO_4)_3$ demonstrates redox reactions of V^{3+}/V^{n+} with 1.5 electrons per unit.[45] Recently, the $Na_3Cr_{0.5}V_{1.5}(PO_4)_3$ cathode material with a high specific capacity of 70 mA h g^{-1} at 1 A g^{-1}[46], was introduced by Goodenough *et al.*[47] This was achieved by leveraging multi-electron reactions involving V^{2+}/V^{3+}, V^{3+}/V^{4+}, and V^{4+}/V^{5+}.[47] Masquelier *et al.* discovered that Al^{3+} is a appropriate positive ion for multi-electron reactions. Additionally, they documented the $Na_3Al_{0.5}V_{1.5}(PO_4)_3$ anode substance, which demonstrated that the introduction of Al^{3+} could initiate the charge/discharge reaction of V^{4+}/V^{5+} at 3.9 V, consequently

[a]College of Chemistry and Chemical Engineering, Shaanxi University of Science and Technology, Xi'an 710021, China. E-mail: liushuling@sust.edu.cn; jianbotong@aliyun.com
[b]Shaanxi Key Laboratory of Chemical Additives for Industry, Xi'an 710021, China
[c]Shaanxi Applied Physics and Chemistry Research Institute, China
[d]State Key Laboratory of Advanced Processing and Recycling of Non-ferrous Metals, Lanzhou University of Technology, Lanzhou 730050, China

enhancing the energy density of the SIB.[48] Nevertheless, all of these doped cations do not exhibit any electrochemical activity, leading to a significant decrease in the specific capacity by unit.[46,48]

From an application perspective, sodium-ion battery cathode materials should ideally possess characteristics such as environmental friendliness and cost-effectiveness. The substantial usage of vanadium in NVP ($Na_3V_2(PO_4)_3$) poses limitations on its sustainable development and large-scale industrial applications. The introduction of iron (Fe) as a dopant is motivated by several factors. Iron is characterized by its electrochemical reactivity, aiming to minimize capacity losses in the battery material. Furthermore, it is non-toxic and economically advantageous, contributing to a more sustainable and cost-effective production process. The present research examines the economical and harmless incorporation of Fe ions exploring the synthesis of a novel cathode material, NFVP/C, with a NASICON structure $Na_3Fe_{0.8}V_{1.2}(PO_4)_3$/C, using the sol–gel technique. We analyze the NFVP's crystal structure and investigate its electrochemical performance in SIB.

2. Experimental

2.1 Synthesis of $Na_3Fe_{0.8}V_{1.2}(PO_4)_3$/C

To synthesize $Na_3Fe_{0.8}V_{1.2}(PO_4)_3$/C, 0.8 mmol of ferric nitrate ($Fe(NO_3)_3\cdot 9H_2O$) and 1.20 mmol of ammonium metavanadate (NH_4VO_3) were added to an aqueous solution of citric acid. The resulting mixture was stirred thoroughly for 30 min at 70 °C in a water bath. Next, 3.1 mmol of sodium acetate (CH_3COONa) and 0.15 g of glucose ($C_6H_80_6$) were added in sequence to the above solution. 3 mmol of ammonium dihydrogen phosphate ($NH_4H_2PO_4$) was gradually added to the solution and stirred for 30 min until a uniform mixture was achieved. Subsequently, 3 mmol of ammonium dihydrogen phosphate ($NH_4H_2PO_4$) were added to the solution while stirring for another 30 min until a homogenous solution was formed. Finally, the solution was heated in a water bath at 80 °C until a gel was formed. The gel retrieved was dried in an oven and ground into powder by using a mortar and pestle. The powder obtained through the sol–gel method underwent a two-step heating process in a tube furnace. In the first step, the powder was heated at 300 °C for 3 hours to eliminate ammonia, water, and carbon dioxide, using carbon dioxide, ammonia, and water in the experiment. After grinding the sample for 2 hours, the second step involved heating the sample at 750 °C for 8 hours under argon protection. The initial heating process had a rate set at 2 °C min^{-1}, followed by 3 °C min^{-1} for the rest of the duration. The sample was then retrieved, resulting in the target product.

Table 1 Crystal data and structure refinement for $Na_3Fe_{0.8}V_{1.2}(PO_4)_3$

Parameter	
Chemical formula	$Na_3Fe_{0.8}V_{1.22}(PO_4)_3$
Space group	$R\bar{3}c$
Step scan increment (°)	0.02
2θ range (°)	5–80
a (Å)	8.717
c (Å)	21.84
V (Å^3)	1437.27
R_{wp}	5.83%
R_p	4.57%

Table 2 Atomic coordinates and equivalent isotropic temperature factors for $Na_3Fe_{0.8}V_{1.2}(PO_4)_3$ at room temperature

Atom	Site	X	Y	Z	Occ
Na (1)	6b	0.33330	0.66670	0.16670	0.134
Na (2)	18e	0.66670	0.96541	0.08330	0.366
V	12c	0.33330	0.66670	0.01895	0.202
Fe	12c	0.33330	0.66670	0.01895	0.125
P	18e	−0.04392	0.33330	0.08330	0.500
O (1)	36f	0.14124	0.49766	0.07922	1.000
O (2)	36f	0.54438	0.84486	−0.02703	1.000

2.2 Material characterization

At room temperature, Cu Kα radiation was used to collect X-ray diffraction (XRD) patterns on a Bruker D8 diffractometer. The structures of the substance were analyzed using a Hitachi SU-8010 microscope through field emission scanning electron microscopy (SEM), while the chemical compositions were examined through energy-dispersive X-ray spectroscopic (EDS) analysis. The XPS analysis was conducted using an ULVAC-PHI PHI-5000 VPIII device equipped with Al Kα radiation, and the XPS-spectra were processed using the Thermo Avantage software.

2.3 Electrochemical measurements

Electrochemical tests were performed using CR2032 coin cells. To form the operational electrode, a mixture of $Na_3Fe_{0.8}V_{1.2}(PO_4)_3$/C samples, acetylene black, and polyvinylidene fluoride was combined in a mass ratio of 8 : 1 : 1. Propylene carbonate (1.0 M) containing $NaClO_4$ was utilized. The electrolyte composition consists of 1 M $NaClO_4$, with PC as the solvent. Additionally, we have incorporated 5% FEC as an additive to enhance performance. The separator employed was a glass fiber diaphragm. Half cells employed self-produced sodium metal foil as the counter electrode.[49] Regarding sodium-ion batteries with symmetrical properties.

2.4 Calculations using density functional theory

The Vienna *ab initio* simulation package (VASP) was used to perform all calculations, which were based on density functional

Table 3 Selected bond distances for $Na_3Fe_{0.8}V_{1.2}(PO_4)_3$

Bond	Distance (Å)	Bond	Distance (Å)
V/Fe–O (1) × 3	2.06	Na (1)–O (1) × 6	2.48
V/Fe–O (2) × 3	1.98	Na (2)–O (1) × 2	2.43
P–O (1) × 2	1.53	Na (2)–O (2) × 2	2.63
P–O (2) × 2	1.50	Na (2)–O (2) × 2	2.81

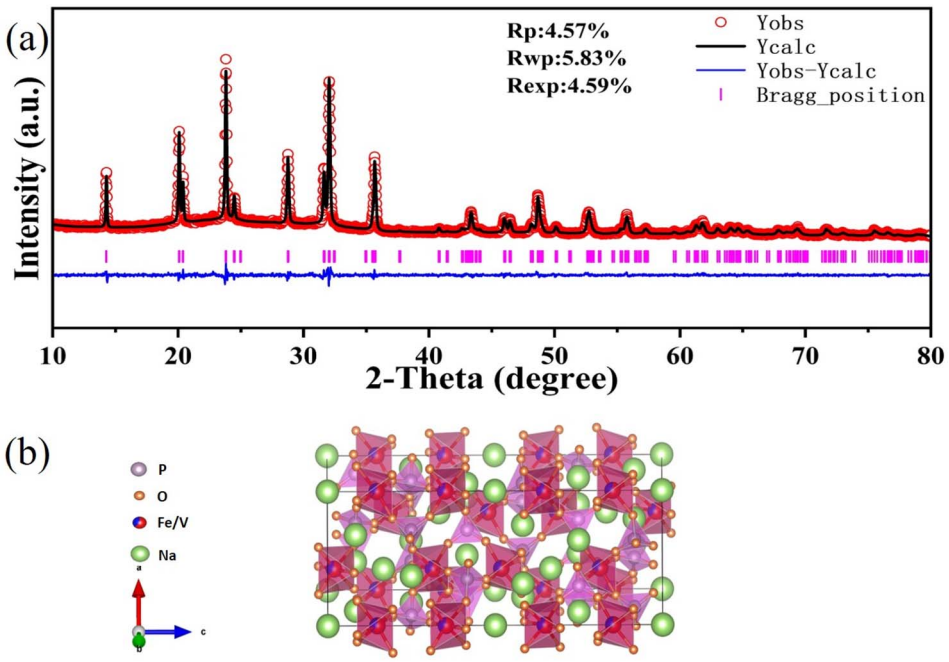

Fig. 1 (a) Rietveld refinement of XRD for $Na_3Fe_{0.8}V_{1.2}(PO_4)_3$/C samples; (b) crystal structure of one unit cell $Na_3Fe_{0.8}V_{1.2}(PO_4)_3$ showing the characteristic "lantern" units.

theory and first-principles calculations. Projected added waves (PAW) describe the interactions between the core separation and valence electrons, while the local density is characterized by the generalized gradient approximation (GGA) which is based on the PBE exchange correlation energy. The Monkhorst–Pack method was utilized to sample the divisions of the Brillouin zone. The calculation used a cutoff energy value of 400 eV, denoted as ENCUT. Optimizing the convergence sampling in the calculation of the diffusion barrier and mechanical strength generated the *K* points of dimensions 1*1*1–3*3*1. Using the elastic energy band method (NEB), the migration routes and energy obstacles of individual lithium ions were computed. The electron and ion relaxation convergence precision values are 1.0×10^{-4} eV and 1.0×10^{-3} eV, respectively, while the force convergence criterion is 0.02 eV $Å^{-1}$.[50]

3. Results and discussion

3.1 Crystal structure of NFVP/C

A straightforward sol–gel method was utilized in the fabrication of NFVP/C samples. After preheating the dried gel at 300 °C, oxalic acid remains. Oxalic acid played a crucial part in the

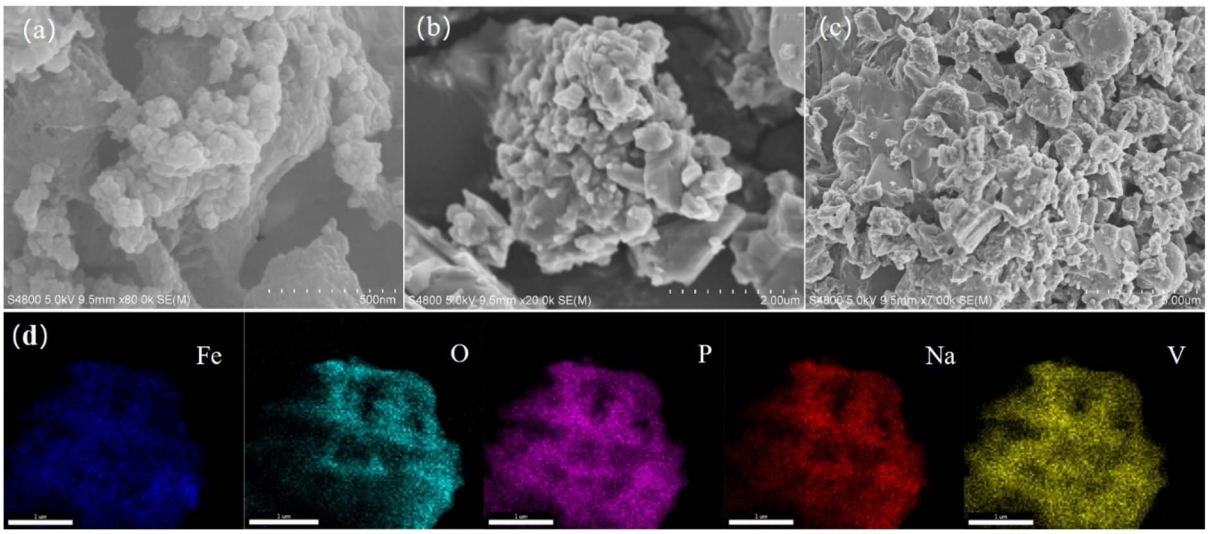

Fig. 2 SEM (a–c), EDS mapping images (d) of the $Na_3Fe_{0.8}V_{1.2}(PO_4)_3$/C samples.

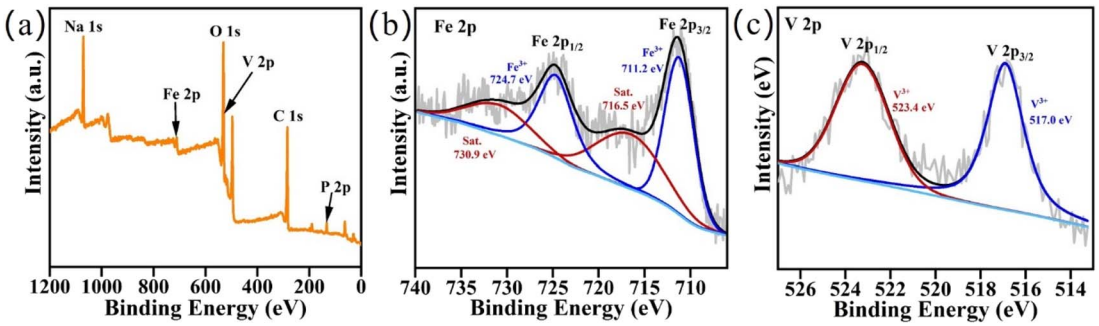

Fig. 3 Wide-range scanning XPS spectra (a) of $Na_3Fe_{0.8}V_{1.2}(PO_4)_3$/C sample and high-resolution spectra of Fe 2p (b) and V 2p (c).

synthesis, acting as a reductive agent, chelator, and source of carbon. The partial breakdown leads to the formation of residual carbon, which remains intact after the subsequent calcination at 700 °C in N_2 and adheres to the surface of NFVP particles, resulting in the creation of NFVP/C. The XRD analysis indicates the NFVP/C is an isostructural with the NASICON-structured compounds. The crystal structure was further confirmed using the GSAS-II software with XRD Rietveld refinement. The crystallographic data supports this conclusion. The data obtained from $Na_2FeTi(PO_4)_3$ (ref. 51) indicates that the refinement process has led to reliability factors of R_{wp} = 5.83% and R_p = 4.57%. The improved findings suggest that NFVP/C can be precisely classified into the $R\bar{3}c$ space group, with unit cell dimensions of $a = 8.717$ (Å), $c = 21.84$ (Å), and $V =$ 1437.27 (Å). Tables 1–3 contain the presented information on refinement details, atomic coordinates, and selected bond distances. The asymmetric unit of $Na_3Fe_{0.8}V_{1.2}(PO_4)_3$/C consists of six atoms that are crystallographically independent. Within this unit, both V and Fe atoms are found at the same 12c sites. There are Na (1) atoms located in 6b sites. Na (2) is fully occupied in 18e sites with partial occupation, and there are also 18e sites where P atoms are located. Furthermore, the general 36f sites contain two O atoms. The bond distances of V/Fe–O, P–O, and Na–O are within an acceptable range and comparable to those found in other compounds with NASICON structure, suggesting the accuracy of the refinement in determining the structure. The crystalline arrangement of a single unit cell of NFVP is depicted in Fig. 1(b). The presence of Na^+ in the cavities demonstrates the formation of a robust and three-dimensional framework through the corner sharing of V/FeO_6 octahedra and PO_4 tetrahedra. The distinguishing feature of NASICONs, $Na_3Fe_{0.8}V_{1.2}(PO_4)_3$, is the presence of "lantern" units.

The morphology and structure information of NFVP/C samples were examined using SEM. The scanning electron microscope (SEM) image reveals that the samples synthesized in their original form consist of non-uniform particles measuring in size 0.5–2 μm

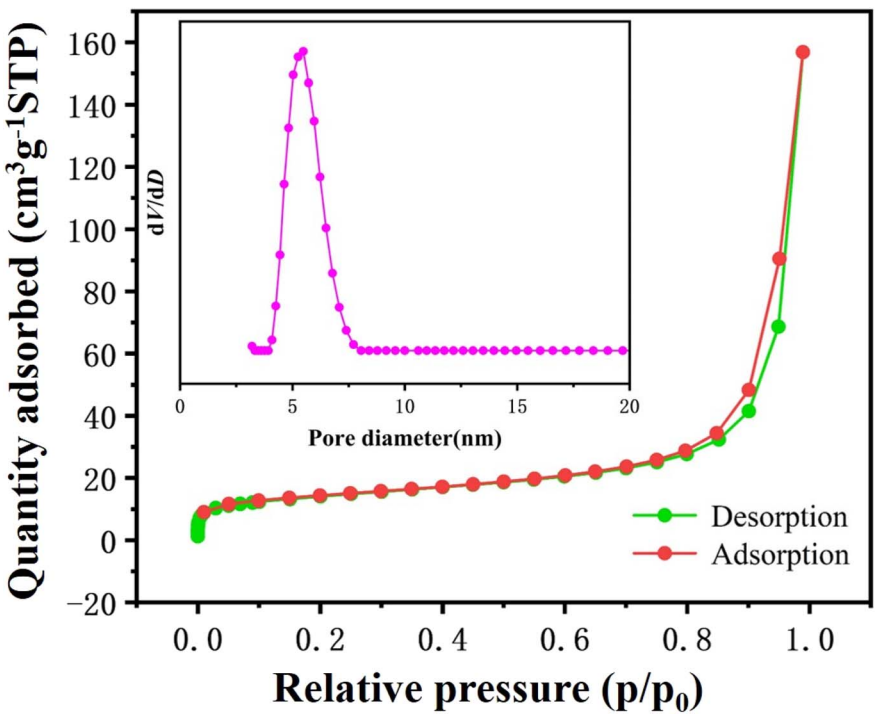

Fig. 4 BET profiles of $Na_3Fe_{0.8}V_{1.2}(PO_4)_3$/C, inset is the distribution of pore size.

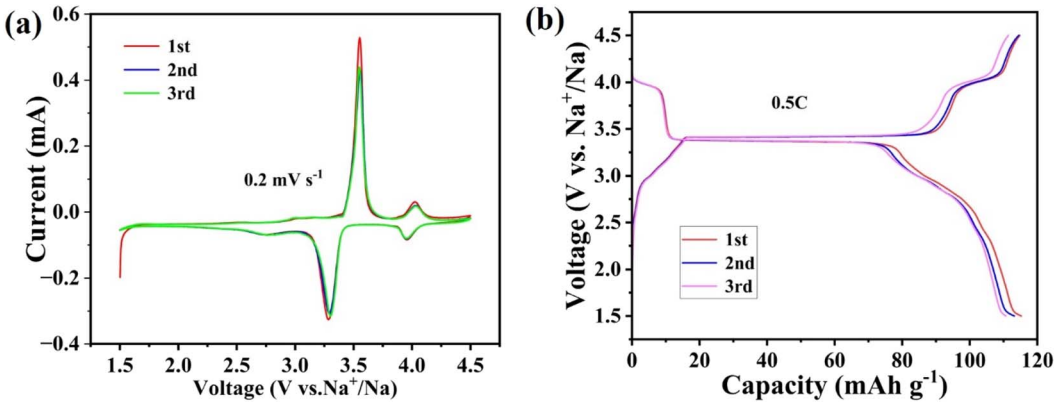

Fig. 5 (a) CV curves at a scan rate of 0.2 mV s^{-1} of the $Na_3Fe_{0.8}V_{1.2}(PO_4)_3$/C cathode within the voltage window of 1.5–4.5 V *versus* Na^+/Na; (b) initial three charge and discharge curves of the Na|| $Na_3Fe_{0.8}V_{1.2}(PO_4)_3$/C cell at 0.5C in the voltage ranges of 1.5–4.5 V.

(Fig. 2(a–c)). The distribution of elements can be analyzed using EDS with scanning electron microscopy (SEM). As demonstrated in Fig. 2(d). The NFVP/C contains a uniform distribution of the elements Na, Fe, V, P, and O. Additionally, the X-ray photoelectron spectroscopy (XPS) analysis of the NFVP/C is shown in Fig. 3. In the analysis, the V peak positions in the fitted XPS are observed at 516.9 eV and 523.7 eV, which correspond to the V $2p_{3/2}$ and V$2p_{1/2}$ peaks of V^{3+}.The fitted XPS peak of Fe is also shown. The peaks at 712.7 eV and 726.4 eV represent the Fe $2p_{3/2}$ and Fe $2p_{1/2}$ peaks of Fe^{3+}, respectively. This suggests that both Fe and V exist in the trivalent state within the NFVP/C. Nitrogen adsorption and desorption tests were conducted on the NFVP/C. As illustrated in the Fig. 4. The nitrogen adsorption and desorption isotherm reveal a swift rise in nitrogen adsorption and desorption between 0.5–0.8 relative air pressure, succeeded by a gradual ascent, indicating a typical type IV curve. The BET method calculates the specific surface area as 58.72 square meters per gram. The figure provided illustrates that the pore size, as determined by the BJH technique, is predominantly approximately 7 nanometers.

3.2 Electrochemical performance of Na||NFVP/C cell

The NFVP/C was studied as the cathode material in an Na||NFVP/C cell to evaluate its electrochemical performance. Fig. 5(a) depicts the Na||NFVP/C cell's charge–discharge profiles. At a current rate of 0.5C, the voltage range is between 1.5 and 4.5 V. During this range, a charging capacity of 114.8 mA h g^{-1} and a discharging capacity of 115.2 mA h g^{-1} are attained, with 1C equivalent to 117 mA h g^{-1}. Even after three cycles, the discharging capacity of 111.4 mA h g^{-1} remains unchanged. Fig. 5(b) outlines the CV curves illustrating two

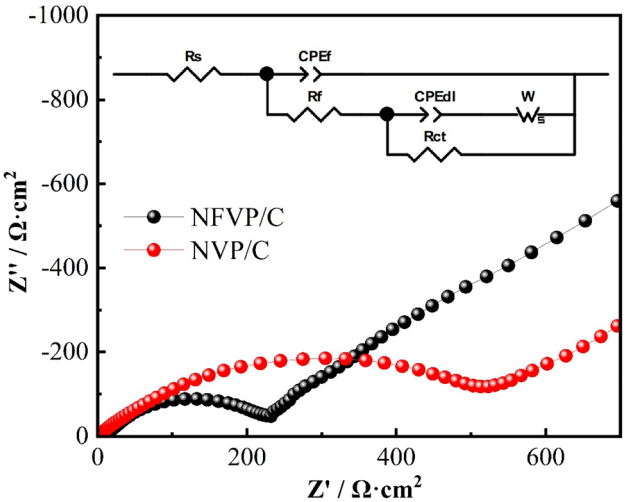

Fig. 7 EIS curves of NVP/C and NFVP/C material.

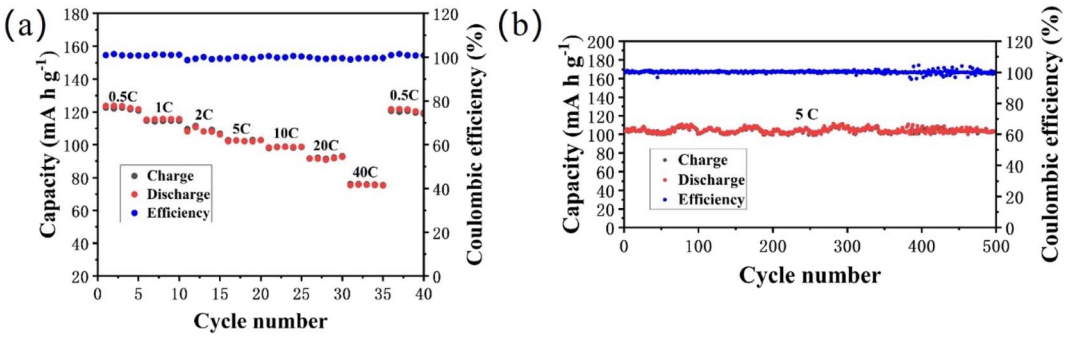

Fig. 6 (a) Rate capability of Na|| $Na_3Fe_{0.8}V_{1.2}(PO_4)_3$/C cell in the voltage ranges of 1.5–4.5 V. (b) Five hundreds cycling performance of Na|| $Na_3Fe_{0.8}V_{1.2}(PO_4)_3$/C cell tested under 5C from 1.5 to 4.5 V.

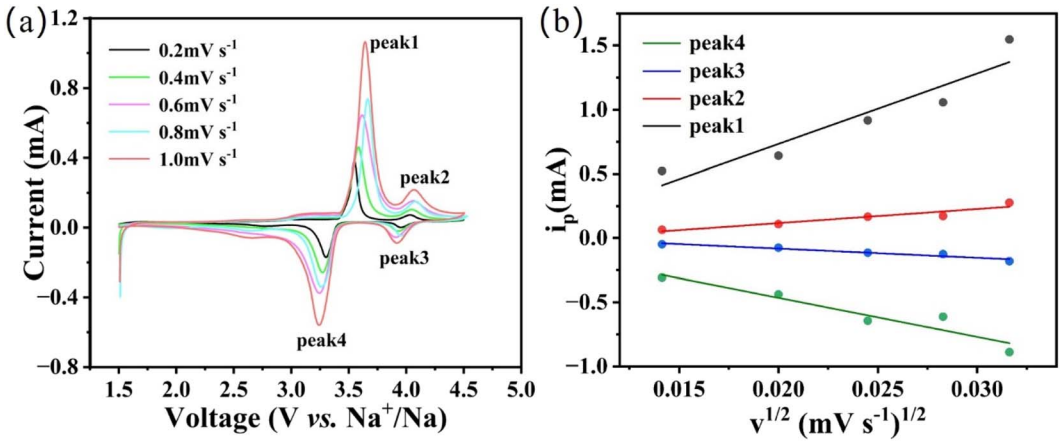

Fig. 8 (a) CV curves at different scanning rates; (b) the relationship between the peak current and the square root of the scan rate.

different reaction platforms at 3.4 V and 4.0 V. After three cycles, the discharge capacity of the sample remains at 111.4 mA h g^{-1}. Fig. 5(b) displays the charge/discharge curves, revealing two separate reaction platforms at 3.4 V and 4.0 V, while the CV curves are shown. Two sets of redox peaks are displayed within the 1.5–4.5 V range. Redox pairs V^{4+}/V^{5+}, V^{3+}/V^{4+}, and V^{3+}/V^{4+} have voltages of 4.03 V/3.95 V and 3.54/3.30 V, respectively. Furthermore, the CV curves for each cycle have a substantial overlap, which confirms a highly reversible electrochemical process. Despite the fact that the introduction of Fe^{3+} decreases the reaction potential, the higher specific capacity and reaction potential of V^{4+}/V^{5+} are advantageous in obtaining a high energy density. Fig. 6(a) shows the evaluation of the rate performance of the Na||NFVP/C cell across a temperature range of 0.5C to 40C. At 0.5C, 1.0C, 2.0C, 5.0C, 10.0C, 20.0C, and 40.0C, the Na||NFVP/C cell demonstrates rate performances of 115.1 mA h g^{-1}, 111.2 mA h g^{-1}, 107.9 mA h g^{-1}, 103 mA h g^{-1}, 98.7 mA h g^{-1}, 90.4 mA h g^{-1}, and 74.2 mA h g^{-1} respectively. Even when reaching 40C, the material maintains a consistent specific capacity. Specific capacities of can still be attained. Even when brought back to 0.5C, it is still possible to attain an impressive specific capacity of 113.0 mA h g^{-1}, demonstrating exceptional structural stability during high rate performance. In comparison with other doped NVP, the rate performance of the current material is exceptional.[44] Fig. 6(b) illustrates the implementation of a comprehensive analysis of a prolonged cycle at a temperature of 5C. Surprisingly, the Na||NFVP/C cell is able to retain 97.8% of its original capacity even after undergoing 500 cycles at 5C. After EIS testing (Fig. 7), the NFVP/C material has a low charge transfer resistance (R_{ct}) and interfacial contact resistance, which indicates that Fe^{+} can significantly improve the electrical conductivity of the composite.

The CV of the Na||NFVP/C cell is shown in Fig. 8(a) for different scan rates between 1.5 and 4.5 V, revealing the presence of two sets of redox peaks that represent the insertion and extraction of Na^{+}. The oxidation–reduction peaks are slightly shifted as the scanning rate increases due to cathode polarization. The linear relationship between the redox peak currents and the square root of the scan rate is depicted in Fig. 8(b). To determine the diffusion coefficient of Na^{+} ions ($D_{Na^{+}}$), one can utilize the Randles–Sevcik equation:[52,53]

$$i_p = 2.69 \times 10^5 A n^{3/2} C_o D^{1/2} v^{1/2}$$

where the peak current is denoted by i_p, and A represents the actual contact area between the electrode sheet and the electrolyte. The electrode reaction involves n electron transfer, while C_o signifies the concentration of sodium ions in the bulk phase. Finally, v refers to the sweep speed. For the peak 1 and peak 4, $D_{Na^{+}}$ is calculated as 5.368×10^{-12} cm^2 s^{-1} and 1.649×10^{-12} cm^2 s^{-1}, respectively. This is one order of magnitude higher than that of $Na_3V_2(PO_4)_3$ (7.19×10^{-13} cm^2 s^{-1}).[49,54]

Fig. 9 summarizes the discharge voltage as a function of specific capacity for the present NFVP material. Not only higher specific capacity but also higher discharge voltage is demanded toward excellent performance of energy density[55–58]

In order to determine the source of the excellent Na-storage performance of NFVP/C, density functional theory (DFT) calculations were conducted to clarify the pathways and

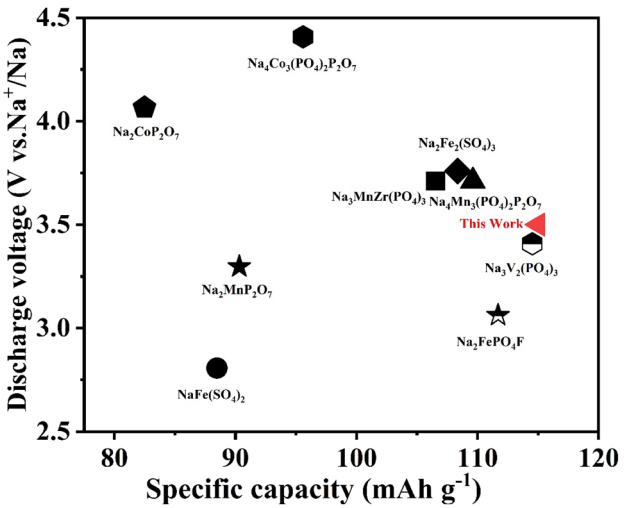

Fig. 9 Comparisons between this work and other developed polyanionic cathode materials for sodium-ion batteries.

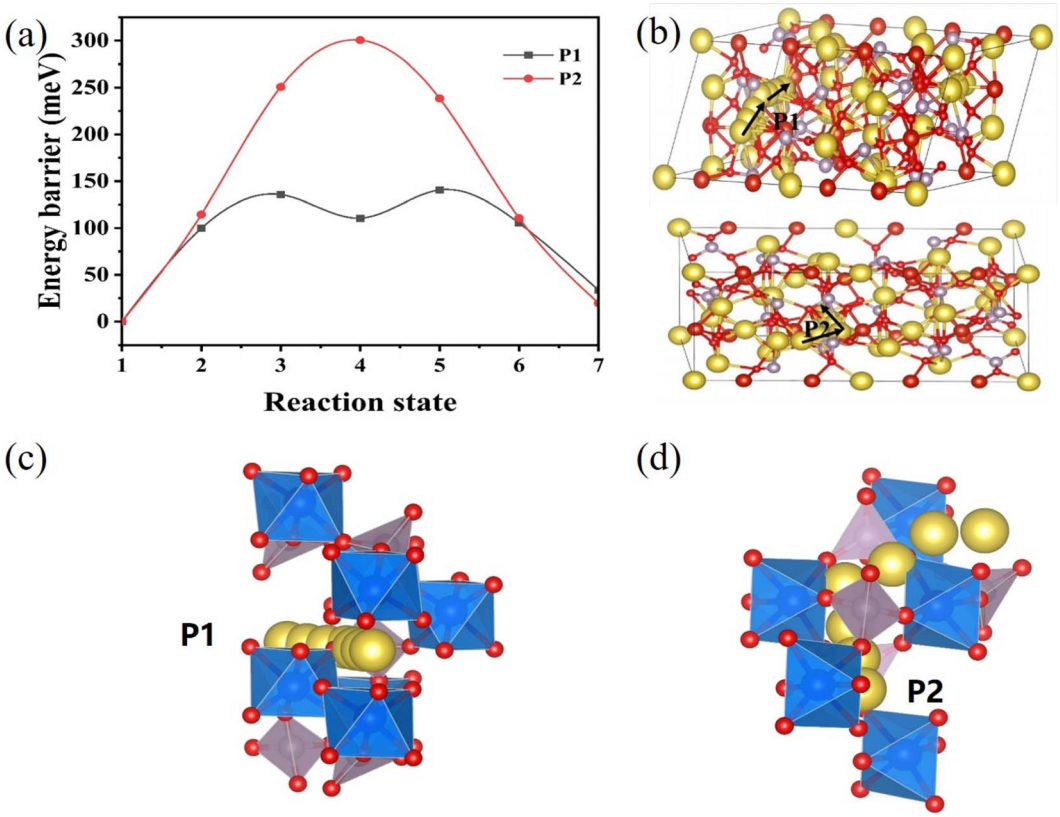

Fig. 10 (a) Corresponding migration energy barriers in the $Na_3Fe_{0.8}V_{1.2}(PO_4)_3$ crystal; (b) possible Na^+ migration pathways, (c and d) are P1 and P2 paths.

obstacles for Na^+ migration. Two potential migration routes, Na → Na (P1), which the migration pathways of Na^+ in the channel between the [PO_4] tetrahedral. Na → Na (P2),That migration pathways of Na^+ in the space between [Fe/VO_6] octahedron. In Fig. 10(a) the energy barriers for the P1 and P2 paths were calculated to be 0.14 eV and 0.30 eV, respectively, using the climbing-image nudged elastic band method.[59] Hence, it is evident that the P1 channels (the upper channel in Fig. 10(b)) running alongside the [$Na_3Fe_{0.8}V_{1.2}(PO_4)_3$] structure offer the most favorable routes for Na^+ diffusion in terms of energy. The migration barrier of 0.14 eV for this is similar to $Na_3V_2(PO_4)_3$, but significantly lower than the migration barriers of the majority of reported cathode materials for SIB.[59] The remarkable response kinetics and favorable rate performance of NFVP can be attributed to the minimal energy barrier for ionic migration.

4. Conclusion

To summarize, the sol–gel method was employed to synthesize a $Na_3Fe_{0.8}V_{1.2}(PO_4)_3$/C phosphate cathode material possessing a NASICON structure. The NASICON structure of $Na_3Fe_{0.8}V_{1.2}(PO_4)_3$/C was confirmed through XRD Rietveld refinement, revealing a unit-cell parameter of $a = 8.717\ (1)$ Å, $c = 21.84\ (1)$ Å, and $V = 1437.27\ (0)$ Å^3. The cyclic voltammetry (CV) of Na||NFVP/C cell exhibits two separate reaction plateaus at 3.4 V and 4.0 V, which correspond to the reversible redox reactions of V^{4+}/V^{5+} and V^{3+}/V^{4+}. After 500 cycles at 5C, the Na||NFVP/C cell achieves a capacity retention rate of 95.3%, with a specific capacity of 115.2 mA h g^{-1} at 5C and 76.4 mA h g^{-1} at 40C. The Na^+ diffusion coefficient of NFVP/C was found to be high, as indicated by the first-principle calculation revealing a low diffusion barrier for Na^+. The findings of this research indicate that the newly discovered substance with NASICON characteristics holds great potential as a suitable contender for storing Na^+ ions.

Conflicts of interest

There are no conflicts to declare.

Acknowledgements

This work was supported by the National Natural Science Foundation of China (22278255) and the Graduate Innovation Fund of Shaanxi University of Science and Technology.

References

1 S. P. Ong, *et al.*, Voltage, stability and diffusion barrier differences between sodium-ion and lithium-ion intercalation materials, *Energy Environ. Sci.*, 2011, **4**, 3680–3688, DOI: 10.1039/c1ee01782a.

2 V. Thangadurai and B. Chen, Solid Li- and Na-Ion Electrolytes for Next Generation Rechargeable Batteries, *Chem. Mater.*, 2022, **34**, 6637–6658, DOI: **10.1021/acs.chemmater.2c01475**.

3 Z. Zhu, *et al.*, Rechargeable Batteries for Grid Scale Energy Storage, *Chem. Rev.*, 2022, **122**, 16610–16751, DOI: **10.1021/acs.chemrev.2c00289**.

4 Lithium-ion batteries need to be greener and more ethical, *Nature*, 2021, **595**, 7, DOI: **10.1038/d41586-021-01735-z**.

5 Y. Feng, *et al.*, Challenges and advances in wide-temperature rechargeable lithium batteries, *Energy Environ. Sci.*, 2022, **15**, 1711–1759, DOI: **10.1039/d1ee03292e**.

6 J. Li, J. Fleetwood, W. B. Hawley and W. Kays, From Materials to Cell: State-of-the-Art and Prospective Technologies for Lithium-Ion Battery Electrode Processing, *Chem. Rev.*, 2022, **122**, 903–956, DOI: **10.1021/acs.chemrev.1c00565**.

7 L. Mauler, F. Duffner, W. G. Zeier and J. Leker, Battery cost forecasting: a review of methods and results with an outlook to 2050, *Energy Environ. Sci.*, 2021, **14**, 4712–4739, DOI: **10.1039/d1ee01530c**.

8 L. P. Wang, L. Yu, X. Wang, M. Srinivasan and Z. J. Xu, Recent developments in electrode materials for sodium-ion batteries, *J. Mater. Chem. A*, 2015, **3**, 9353–9378, DOI: **10.1039/c4ta06467d**.

9 Y. Huang, *et al.*, Electrode Materials of Sodium-Ion Batteries toward Practical Application, *ACS Energy Lett.*, 2018, **3**, 1604–1612, DOI: **10.1021/acsenergylett.8b00609**.

10 J. Xiao, *et al.*, Recent progress of emerging cathode materials for sodium ion batteries, *Mater. Chem. Front.*, 2021, **5**, 3735–3764, DOI: **10.1039/d1qm00179e**.

11 X. Xiang, K. Zhang and J. Chen, Recent Advances and Prospects of Cathode Materials for Sodium-Ion Batteries, *Adv. Mater.*, 2015, **27**, 5343–5364, DOI: **10.1002/adma.201501527**.

12 N. Yabuuchi, K. Kubota, M. Dahbi and S. Komaba, Research development on sodium-ion batteries, *Chem. Rev.*, 2014, **114**, 11636–11682, DOI: **10.1021/cr500192f**.

13 Y. Li, *et al.*, Recent advances of electrode materials for low-cost sodium-ion batteries towards practical application for grid energy storage, *Energy Storage Mater.*, 2017, **7**, 130–151, DOI: **10.1016/j.ensm.2017.01.002**.

14 H. Hou, C. E. Banks, M. Jing, Y. Zhang and X. Ji, Carbon Quantum Dots and Their Derivative 3D Porous Carbon Frameworks for Sodium-Ion Batteries with Ultralong Cycle Life, *Adv. Mater.*, 2015, **27**, 7861–7866, DOI: **10.1002/adma.201503816**.

15 Y. Wu and Y. Yu, 2D material as anode for sodium ion batteries: Recent progress and perspectives, *Energy Storage Mater.*, 2019, **16**, 323–343, DOI: **10.1016/j.ensm.2018.05.026**.

16 W. J. Li, *et al.*, Commercial Prospects of Existing Cathode Materials for Sodium Ion Storage, *Adv. Energy Mater.*, 2017, **7**, 1700274, DOI: **10.1002/aenm.201700274**.

17 Y. Fang, *et al.*, Phosphate Framework Electrode Materials for Sodium Ion Batteries, *Adv. Sci.*, 2017, **4**, 1600392, DOI: **10.1002/advs.201600392**.

18 N. Ortiz-Vitoriano, N. E. Drewett, E. Gonzalo and T. Rojo, High performance manganese-based layered oxide cathodes: overcoming the challenges of sodium ion batteries, *Energy Environ. Sci.*, 2017, **10**, 1051–1074, DOI: **10.1039/c7ee00566k**.

19 S. Guo, *et al.*, A layered P2- and O3-type composite as a high-energy cathode for rechargeable sodium-ion batteries, *Angew Chem. Int. Ed. Engl.*, 2015, **54**, 5894–5899, DOI: **10.1002/anie.201411788**.

20 P. F. Wang, *et al.*, Suppressing the P2-O2 Phase Transition of $Na_{0.67}Mn_{0.67}Ni_{0.33}O_2$ by Magnesium Substitution for Improved Sodium-Ion Batteries, *Angew Chem. Int. Ed. Engl.*, 2016, **55**, 7445–7449, DOI: **10.1002/anie.201602202**.

21 Q. Wang, *et al.*, Experience and inspirations of the Mass Drug Administration Programme with artemisinin-piperaquine in Moheli Island of the Comoros assisted by China, *J. Commun. Healthcare*, 2018, **2**, 1–7, DOI: **10.1016/s2414-6447(19)30156-3**.

22 Y. Liu, *et al.*, Approaching the Downsizing Limit of Maricite $NaFePO_4$ toward High-Performance Cathode for Sodium-Ion Batteries, *Adv. Funct. Mater.*, 2018, **28**, 1801917, DOI: **10.1002/adfm.201801917**.

23 Y. U. Park, *et al.*, A new high-energy cathode for a Na-ion battery with ultrahigh stability, *J. Am. Chem. Soc.*, 2013, **135**, 13870–13878, DOI: **10.1021/ja406016j**.

24 X. Pu, *et al.*, $Na_4Fe_3(PO_4)_2P_2O_7$/C nanospheres as low-cost, high-performance cathode material for sodium-ion batteries, *Energy Storage Mater.*, 2019, **22**, 330–336, DOI: **10.1016/j.ensm.2019.02.017**.

25 J. Z. Guo, *et al.*, High-Energy/Power and Low-Temperature Cathode for Sodium-Ion Batteries: In Situ XRD Study and Superior Full-Cell Performance, *Adv. Mater.*, 2017, **29**, 1701968, DOI: **10.1002/adma.201701968**.

26 J. Zhao, *et al.*, Moving to Aqueous Binder: A Valid Approach to Achieving High-Rate Capability and Long-Term Durability for Sodium-Ion Battery, *Adv. Sci.*, 2018, **5**, 1700768, DOI: **10.1002/advs.201700768**.

27 P. Barpanda, *et al.*, $Na_2FeP_2O_7$: A Safe Cathode for Rechargeable Sodium-ion Batteries, *Chem. Mater.*, 2013, **25**, 3480–3487, DOI: **10.1021/cm401657c**.

28 Y. Liu, *et al.*, Sodium storage in Na-rich Na x $FeFe(CN)_6$ nanocubes, *Nano Energy*, 2015, **12**, 386–393, DOI: **10.1016/j.nanoen.2015.01.012**.

29 Y. Jiang, *et al.*, Prussian Blue@C Composite as an Ultrahigh-Rate and Long-Life Sodium-Ion Battery Cathode, *Adv. Funct. Mater.*, 2016, **26**, 5315–5321, DOI: **10.1002/adfm.201600747**.

30 S. Wang, *et al.*, All organic sodium-ion batteries with $Na_4C_8H_2O_6$, *Angew Chem. Int. Ed. Engl.*, 2014, **53**, 5892–5896, DOI: **10.1002/anie.201400032**.

31 Z. Jian, *et al.*, Superior Electrochemical Performance and Storage Mechanism of $Na_3V_2(PO_4)_3$ Cathode for Room-Temperature Sodium-Ion Batteries, *Adv. Energy Mater.*, 2013, **3**, 156–160, DOI: **10.1002/aenm.201200558**.

32 S. Li, *et al.*, Effect of carbon matrix dimensions on the electrochemical properties of $Na_3V_2(PO_4)_3$ nanograins for high-performance symmetric sodium-ion batteries, *Adv. Mater.*, 2014, **26**, 3545–3553, DOI: **10.1002/adma.201305522**.

33 X. Zhang, *et al.*, $Na_3V_2(PO_4)_3$: an advanced cathode for sodium-ion batteries, *Nanoscale*, 2019, **11**, 2556–2576, DOI: 10.1039/c8nr09391a.

34 G. L. Xu, *et al.*, Challenges in Developing Electrodes, Electrolytes, and Diagnostics Tools to Understand and Advance Sodium-Ion Batteries, *Adv. Energy Mater.*, 2018, **8**, 1702403, DOI: 10.1002/aenm.201702403.

35 X. Rui, W. Sun, C. Wu, Y. Yu and Q. Yan, An Advanced Sodium-Ion Battery Composed of Carbon Coated $Na_3V_2(PO_4)_3$ in a Porous Graphene Network, *Adv. Mater.*, 2015, **27**, 6670–6676, DOI: 10.1002/adma.201502864.

36 C. Zhu, K. Song, P. A. van Aken, J. Maier and Y. Yu, Carbon-coated $Na_3V_2(PO_4)_3$ embedded in porous carbon matrix: an ultrafast Na-storage cathode with the potential of outperforming Li cathodes, *Nano Lett.*, 2014, **14**, 2175–2180, DOI: 10.1021/nl500548a.

37 Y. Fang, L. Xiao, X. Ai, Y. Cao and H. Yang, Hierarchical carbon framework wrapped $Na_3V_2(PO_4)_3$ as a superior high-rate and extended lifespan cathode for sodium-ion batteries, *Adv. Mater.*, 2015, **27**, 5895–5900, DOI: 10.1002/adma.201502018.

38 T. Jin, *et al.*, Polyanion-type cathode materials for sodium-ion batteries, *Chem. Soc. Rev.*, 2020, **49**, 2342–2377, DOI: 10.1039/c9cs00846b.

39 M. J. Aragón, P. Lavela, R. Alcántara and J. L. Tirado, Effect of aluminum doping on carbon loaded $Na_3V_2(PO_4)_3$ as cathode material for sodium-ion batteries, *Electrochim. Acta*, 2015, **180**, 824–830, DOI: 10.1016/j.electacta.2015.09.044.

40 R. Klee, P. Lavela, M. J. Aragón, R. Alcántara and J. L. Tirado, Enhanced high-rate performance of manganese substituted $Na_3V_2(PO_4)_3$/C as cathode for sodium-ion batteries, *J. Power Sources*, 2016, **313**, 73–80, DOI: 10.1016/j.jpowsour.2016.02.066.

41 H. Li, *et al.*, Understanding the Electrochemical Mechanisms Induced by Gradient Mg^{2+} Distribution of Na-Rich $Na^{3+x}V_{2-x}Mg_x(PO_4)_3$/C for Sodium Ion Batteries, *Chem. Mater.*, 2018, **30**, 2498–2505, DOI: 10.1021/acs.chemmater.7b03903.

42 X. Li, *et al.*, High valence Mo-doped $Na_3V_2(PO_4)_3$/C as a high rate and stable cycle-life cathode for sodium battery, *J. Mater. Chem. A*, 2018, **6**, 1390–1396, DOI: 10.1039/c7ta08970h.

43 X. Liu, *et al.*, Insight into Preparation of Fe-Doped $Na_3V_2(PO_4)_3$@C from Aspects of Particle Morphology Design, Crystal Structure Modulation, and Carbon Graphitization Regulation, *ACS Appl. Mater. Interfaces*, 2019, **11**, 12421–12430, DOI: 10.1021/acsami.8b21257.

44 Y. Huang, *et al.*, Superior Na-ion storage achieved by Ti substitution in $Na_3V_2(PO_4)_3$, *Energy Storage Mater.*, 2018, **15**, 108–115, DOI: 10.1016/j.ensm.2018.03.021.

45 R. Liu, *et al.*, Exploring Highly Reversible 1.5-Electron Reactions ($V_{3+}/V_{4+}/V_{5+}$) in $Na_3VCr(PO_4)_3$ Cathode for Sodium-Ion Batteries, *ACS Appl. Mater. Interfaces*, 2017, **9**, 43632–43639, DOI: 10.1021/acsami.7b13018.

46 X. Min, *et al.*, Potassium-ion batteries: outlook on present and future technologies, *Energy Environ. Sci.*, 2021, **14**, 2186–2243, DOI: 10.1039/d0ee02917c.

47 Y. Zhao, X. Gao, H. Gao, H. Jin and J. B. Goodenough, Three Electron Reversible Redox Reaction in Sodium Vanadium Chromium Phosphate as a High-Energy-Density Cathode for Sodium-Ion Batteries, *Adv. Funct. Mater.*, 2020, **30**, 1908680, DOI: 10.1002/adfm.201908680.

48 F. Lalère, *et al.*, Improving the energy density of $Na_3V_2(PO_4)_3$-based positive electrodes through V/Al substitution, *J. Mater. Chem. A*, 2015, **3**, 16198–16205, DOI: 10.1039/c5ta03528g.

49 L. Li, Y. Jia, L. Song and J. Gao, $Na_2VS_n(PO_4)_3$: A novel NASICON-type electrode material for symmetric sodium-ion batteries, *J. Alloys Compd.*, 2023, **942**, 169128, DOI: 10.1016/j.jallcom.2023.169128.

50 Y. Ren, *et al.*, Effect of the mechanical strength on the ion transport in a transition metal lithium halide electrolyte: first-principle calculations, *Mater. Today Commun.*, 2022, **33**, 104570, DOI: 10.1016/j.mtcomm.2022.104570.

51 S. Patoux, G. Rousse, J.-B. Leriche and C. Masquelier, Structural and Electrochemical Studies of Rhombohedral $Na_2TiM(PO_4)_3$ and $Li_{1.6}Na_{0.4}TiM(PO_4)$= (M: Fe, Cr) Phosphates, *ChemInform*, 2003, **34**, DOI: 10.1002/chin.200334012.

52 N. Yabuuchi and S. Komaba, Recent research progress on iron- and manganese-based positive electrode materials for rechargeable sodium batteries, *Sci. Technol. Adv. Mater.*, 2014, **15**, 043501, DOI: 10.1088/1468-6996/15/4/043501.

53 V. L. McLaren, *et al.*, Study of the Capacity Fading Mechanism for Fe-Substituted LiCoO[sub 2] Positive Electrode, *J. Electrochem. Soc.*, 2004, **151**, A672, DOI: 10.1149/1.1688796.

54 X. Li, *et al.*, Jahn–Teller Assisted Na Diffusion for High Performance Na Ion Batteries, *Chem. Mater.*, 2016, **28**, 6575–6583, DOI: 10.1021/acs.chemmater.6b02440.

55 X. Rui, *et al.*, NASICON Electrodes: A Low-Temperature Sodium-Ion Full Battery: Superb Kinetics and Cycling Stability, *Adv. Funct. Mater.*, 2021, **31**, 2170070, DOI: 10.1002/adfm.202170070.

56 W. Shen, C. Wang, H. Liu and W. Yang, Towards highly stable storage of sodium ions: a porous $Na_3V_2(PO_4)_3$/C cathode material for sodium-ion batteries, *Chemistry*, 2013, **19**, 14712–14718, DOI: 10.1002/chem.201300005.

57 J. Kim, G. Yoon, H. Kim, Y.-U. Park and K. Kang, Na3V(PO4)2: A New Layered-Type Cathode Material with High Water Stability and Power Capability for Na-Ion Batteries, *Chem. Mater.*, 2018, **30**, 3683–3689, DOI: 10.1021/acs.chemmater.8b00458.

58 S. Xu, *et al.*, Vanadium fluorophosphates: advanced cathode materials for next-generation secondary batteries, *Mater. Horiz.*, 2023, **10**, 1901–1923, DOI: 10.1039/d3mh00003f.

59 M. Chen, *et al.*, NASICON-type air-stable and all-climate cathode for sodium-ion batteries with low cost and high-power density, *Nat. Commun.*, 2019, **10**, 1480, DOI: 10.1038/s41467-019-09170-5.